ACS APPLIED MATERIALS & INTERFACES

Article

Facile synthesis of potassium poly(heptazine imide) (PHIK) / Ti-based Metal-Organic Framework (MIL-125-NH) composites for photocatalytic applications

Nicolás Artemio Rodríguez, Aleksandr Savateev, Maria Alejandra Grela, and Dariya Dontsova

ACS Appl. Mater. Interfaces, **Just Accepted Manuscript** • Publication Date (Web): 13 Jun 2017

Just Accepted

ACS Publications

ACS Applied Materials & Interfaces is published by the American Chemical Society.
1155 Sixteenth Street N.W., Washington, DC 20036

Facile synthesis of potassium poly(heptazine imide) (PHIK) / Ti-based Metal-Organic Framework (MIL-125-NH_2) composites for photocatalytic applications

Nicolás A. Rodríguez[1,2], Aleksandr Savateev[3], María A. Grela[1,2], Dariya Dontsova[3*]*

[1]Departamento de Química, Facultad de Ciencias Exactas y Naturales (FCEyN), Universidad Nacional de Mar del Plata (UNMdP), 7600 Mar del Plata, Argentina.

[2]Instituto de Física de Mar del Plata (IFIMAR), FCEyN, UNMdP – CONICET, 7600 Mar del Plata, Argentina.

[3]Department of Colloid Chemistry, Max Planck Institute of Colloids and Interfaces, 14476 Potsdam, Germany.

KEYWORDS: Carbon nitride, Metal-Organic Framework, poly(heptazine imide), MIL-125-NH_2, Composite, Photocatalysis, photochromic effect

ABSTRACT. Photocatalytically active composites comprising potassium poly(heptazine imide) (PHIK) and a Ti-based Metal-Organic Framework (MOF, MIL-125-NH_2) are prepared *in-situ* by simply dispersing both materials in water. The driving forces of composite formation are the electrostatic interactions between the solids and the diffusion of potassium ions from PHIK to MIL-125-NH_2. This mechanism implies that other composites of poly(heptazine imide) salts and

different MOFs bearing positive surface charge can potentially be obtained in a similar fashion. The suggested strategy thus opens a new avenue for the facile synthesis of such materials. The composites are shown to have a superior photocatalytic activity in Rhodamine B degradation under visible light irradiation. The reaction rate is doubled compared to that of pure MOF compound and is seven times higher than the activity of the pristine PHIK. The results of the Electron Paramagnetic Resonance (EPR) investigations and the analysis of the electronic structures of the solids suggest the electron transfer from MIL-125-NH_2 to PHIK in the composite. The possible pathways for the dye degradation and the rationalization of the increased activity of the composites are elaborated.

INTRODUCTION

The synthesis of composite materials is an area of much interest in photocatalysis, since the presence of different functional materials facilitates charge separation inducing charge carrier transfer between the components that enhances photocatalytic and photoelectrochemical efficiencies of the integral system.[1,2]

Many materials have been tested in the synthesis of composites. In particular, there is a recent interest in graphitic carbon nitrides (g-CN) / Metal-Organic Frameworks (MOF) heterostructures.[3–5] Carbon nitrides are polymeric metal-free semiconductors extensively studied for photocatalytic applications.[6–8] One of the main advantages of carbon nitrides is that they absorb a high energy fraction of the visible light, however, they typically have low surface areas and are characterized by high charge carrier recombination rates.[9] g-CN is usually obtained by heating cyanamide[4]/dicyanamide[3,5] under inert atmosphere at high temperatures (550°C). However, it has been reported that related polymers with better photocatalytic activities are

obtained by heating substituted 1,2,4-triazole derivatives in LiCl/KCl eutectics. Such a procedure leads to the formation of a carbon nitride polymer salt composed of layers of poly(heptazine imide) with K^+ ions within the interstices.[9] MOFs are hybrid coordination polymers whose optical and electronic properties can be tuned, e.g. by changing an organic or inorganic precursor to obtain isoreticular materials.[10,11] ZIF-9[4,5] and MIL-125[3] have been employed to produce carbon nitride containing composites in order to benefit from the high CO_2 adsorption capability of ZIF-9, and the additional catalytically active titanium centers of MIL-125, respectively. MIL-125-NH_2 is isoreticular to MIL-125, but the replacement of terephthalic acid by aminoterephthalic acid leads to the decrease of the material bandgap and higher retention of CO_2.[11,12]

In general, the synthesis of composites is not straightforward and depends on the properties of the individual components. Possible strategies for the synthesis of metal oxides deposited on other semiconductors are pulsed laser deposition,[13] chemical vapor deposition,[14] etc. Using these approaches it is possible to deposit nanometric particles over films or micrometric structures. Solvothermal synthesis under controlled conditions[15] is also suitable to obtain composites. However, PHIK and MIL-125-NH_2 are both obtained as micrometric particles.[9,11] That makes it more difficult to ensure the crystallization of one material over the other. Many proposed routes in such cases involve a sol-gel synthesis in which a powder is dispersed in a sol of the reagents needed to synthesize the second material. This is especially feasible for metal oxides and TiO_2 in particular.[16–19] Other possibility is to obtain the desired composite by the impregnation technique,[20] as reported by Zhou *et al.* to prepare a g-CN/ ZIF-9 composite.[5]

In this work, a simple and straightforward way to prepare PHIK/MIL-125-NH_2 composites with enhanced photocatalytic activity is reported. The suggested strategy involves only the

dispersion of both materials in water. The analysis of the surface ζ-potentials of the pure solids shows that the components can attract each other by means of electrostatic forces. The comparative analysis of FTIR and photoluminescence spectra, together with the morphological changes observed by SEM proves the formation of a composite. The possible influence of the migration of K^+ ions from PHIK to MIL-125-NH_2 within the composite is discussed. The superior photocatalytic activity of the composite compared to pure semiconductors is exemplified in Rhodamine B (RhB) degradation. EPR studies and Mott-Schottky analysis are used to reveal the electronic structure of the composite. Based on these findings, possible pathways for Rhodamine B degradation are discussed. We suggest that the charge transfer from MIL-125-NH_2 to PHIK is responsible for the increase of Rhodamine B photodegradation rates in the presence of composites as compared to pure materials.

MATERIALS AND METHODS

Chemicals. LiCl (99%, Roth), KCl (99%, Sigma-Aldrich), 3-amino-1,2,4-triazole-5-thiol (98%, Alfa Aesar), N,N-dimethylformamide (DMF, 99.8%, Sigma-Aldrich), acetonitrile (99.9 %, Merck), methanol (99.9%, Merck), titanium (IV) isopropoxide (97 %, Aldrich), pivalic acid (99%, Roth), 2-aminoterephthalic acid (97%, Aldrich), sodium sulfate (99%, Acros Organics) and Rhodamine B (95 %, Sigma Aldrich) were used as received.

Synthesis of the materials. PHIK was prepared by a salt melt synthesis described previously.[9] In a typical procedure, 3 g of 3-amino-1,2,4-triazole-5-thiol were grinded with 6.75 g of LiCl and 8.25 g of KCl in a mortar. The mixture was transferred to a crucible and heated under nitrogen flow (15 $L \cdot min^{-1}$) to 550 °C at a rate of 2.3 $°C \cdot min^{-1}$, then held at 550 °C for 4h. After cooling down, the product was washed with the deionized (DI) water for 12 h, then filtered and washed

three more times with DI water. The humid solid was dried in a vacuum oven overnight (50 °C, 10 mbar).

MIL-125-NH_2 was prepared according to the method reported by Hendon *et al.*[11] The first step involves the solvothermal synthesis of a Ti-based oxocluster $Ti_8O_8(OOCC(CH_3)_3)_{16}$. For that purpose, a solution of 3.2 ml of titanium (IV) isopropoxide and 11.8 g of pivalic acid in 40 ml of acetonitrile was heated at 120 °C during 72 h in a PARR reactor. The product was washed three times with acetonitrile. Finally, 1 g of the oxocluster and 1.3 g of 2-aminoterephthalic acid were dissolved in a mixture of 58 ml of DMF and 18 ml of MeOH. The solution was heated at 120 °C during 72 h in a Teflon-lined PARR reactor. The solid was centrifuged and washed three times with DMF and two times with MeOH, and then dried under vacuum.

Composite materials were prepared *in-situ* by mixing fixed amounts of the pure materials and dispersing the mixture in water. Composites designated as COM25, COM50, COM75 contained 25 wt.%, 50 wt.% and 75 wt.% of PHIK, respectively. For the analysis of the composite, the dispersion was dried under vigorous stirring at room temperature. For comparison purposes, a mixture of PHIK and MIL-125-NH_2 of the same composition as COM50 was prepared. The mixture (MIX50) was not dispersed in water to avoid the formation of the composite.

Characterization. Powder X-Ray diffraction (PXRD) patterns were measured on a Bruker D8 Advance diffractometer equipped with a scintillation counter detector with Cu-Kα radiation (λ = 0.15418 nm). FTIR spectra were acquired on a Varian1000 FTIR spectrometer equipped with an attenuated total reflection (ATR) unit. Nitrogen adsorption/desorption measurements were performed after degassing the samples at 150 °C for 20 h using a Quantachrome Quadrasorb SI-MP porosimeter at 77.4 K. Scanning electron microscopy (SEM) images were obtained on a

LEO 1550-Gemini microscope. Optical absorbance spectra of powders were measured on a Shimadzu UV 2600 spectrophotometer equipped with an integrating sphere. The absorption spectra of RhB solutions were recorded on a T70 UV/VIS spectrophotometer (PG instruments Ltd.). Zeta-potentials were measured in aqueous dispersions of the solids using a Malvern Zetasizer instrument. Mott-Schottky analysis of MIL-125-NH_2 was performed using a film of the solid. The film was prepared by spin-coating (using a Laurell WS400-E spin processor) of an ethanolic dispersion (8 $g \cdot L^{-1}$) on a fluorine doped thin oxide (FTO) glass. The film was immersed in a 0.5 M Na_2SO_4 aqueous solution. The impedance spectroscopy analysis was performed with a Voltalab 40 instrument at a frequency of 1 kHz, using a Pt-cable and a saturated calomel electrode as working and reference electrodes, respectively. N_2 adsorption/desorption isotherms were measured at 77.4 K on a Quadrasorb SI-MP-20 porosimeter (Quantachrome Instruments) after degassing the samples at 150 °C for 20 hours. The specific surface areas were calculated by applying the Brunauer-Emmett-Teller (BET) model to adsorption isotherms at $0.05 < p/p_0 < 0.3$ using the QuadraWin 5.05 software package. The pore size distribution was calculated by the nonlocal density functional theory (NLDFT) method.

Three sets of EPR spectra were obtained at room temperature using a Bruker ELEXSYS E500T spectrometer operating at the X-band. The first set consists of EPR spectra of solid PHIK and COM50 samples, which were smoothed using a fast Fourier transform filter for the sake of clarity. The samples for the second set were prepared by placing different amounts of MIL-125-NH_2 and COM50 (4 and 8 mg, respectively, to ensure the amount of MOF is the same) in an EPR tube, and adding 10 µl of a TEOA solution (20% in acetonitrile) purged with N_2. The tubes were irradiated with a blue LED emitting at 470 nm (3W, LUXEON III – Philips) for 2 h and

then analyzed. The third set was prepared as the second one but employing PHIK and COM50 (1.5 and 3.0 mg, respectively, to provide similar quantities of PHIK in both samples) with 10 µl of the purged TEOA solution. The samples were irradiated with LEDs emitting at 470 and 530 nm (3W, LUXEON III – Philips) for 30 minutes.

Photocatalytic Rhodamine B degradation. 5 mg of the photocatalyst (pure PHIK, MIL-125-NH_2 or a composite) were dispersed in 5 ml of a 100 $mg \cdot L^{-1}$ aqueous solution of RhB. The resulting dispersion was stirred for 2 hours in the dark to allow the adsorption of the dye (and the formation of the composite when a mixture of MIL-125-NH_2 and PHIK was employed). Then the dispersion was irradiated with a blue LED lamp emitting at 465 nm (30 W, OSA Opto Lights). Aliquots of 200 µl of the irradiated dispersion were taken at different irradiation times, then centrifuged and finally diluted with 2.3 mL of DI water. The solutions were then analyzed by UV-Visible light spectrometry to follow the decay of RhB concentration as a function of irradiation time.

Determination of the photon flux through the reactor and apparent quantum efficiencies. A screw-capped tube was charged with the solution of potassium ferrioxalate (5 mL, 150 $mmol \cdot L^{-1}$) and irradiated with a blue LED (40 W, 465 nm) for 15 s. Solution aliquot (1 mL) was transferred into a beaker, phenanthroline solution (4 mL, 1 $mg \cdot mL^{-1}$) and water (20 mL) were added. The procedure was repeated 3 times and the average absorbance (A_{av}) at 510 nm was calculated. A solution for absorption spectrum baseline correction was prepared by mixing potassium ferrioxalate (1 mL, 150 $mmol \cdot L^{-1}$), phenanthroline solution (4 mL, 1 $mg \cdot mL^{-1}$) and water (20 mL). The flux of photons (Q_f) through the reactor was calculated using the equation:

$$Q_f = \frac{A_{av} \cdot V_t \cdot V_r \cdot 60 \cdot 1000}{\varepsilon \cdot l \cdot V_a \cdot 10^3 \cdot QE \cdot \tau} = \frac{1.263 \cdot 25 \cdot 5 \cdot 60 \cdot 1000}{11100 \cdot 1 \cdot 1 \cdot 10^3 \cdot 0.85 \cdot 15} = 0.06693 \quad (1)$$

where Q_f – flux of photons through the reactor, mmol·min^{-1}; A_{av} – Fe^{2+}/phenantroline complex absorption; ε – extinction coefficient, L·mol^{-1}·cm^{-1}; l – cuvette length, cm; V_a – aliquot volume, mL; V_t – total volume, mL; V_r – reaction mixture volume, mL; QE – quantum efficiency of the potassium ferrioxalate photoreduction; τ – irradiation time, s.

Apparent quantum efficiency of the material in a given process can be written as:[21]

$$\varphi_x = \frac{\mp(d[x]dt)}{d[hv]_{inc}/dt} \quad (2)$$

where d[x]/dt is the rate of change of the concentration of the reactant (or product) and d$[hv]_{inc}$/dt is the total optical power impinging on the sample.

Apparent quantum efficiencies of the photocatalysts were calculated assuming that degradation of Rhodamine B chromophore (absorbing at 554 nm) is a one electron/hole process (which is, of course, not true, and a number of the electrons/holes participating in dye degradation is much higher in reality). Equation (2) was then rewritten as:

$$\varphi_x = \frac{\mp(d[x]dt)}{\frac{d[hv]_{inc}}{dt}} = \frac{n_{RhB}}{n_{photon}} = \frac{n_0 - n}{Q_f \cdot 10^{-3} \cdot \tau} = \frac{C_0 \cdot V/M_{RhB} - C \cdot V/M_{RhB}}{Q_f \cdot 10^{-3} \cdot \tau} = \frac{V \cdot (C_0 - C_0 \cdot e^{-k \cdot \tau})}{M_r \cdot Q_f \cdot 10^{-3} \cdot \tau} = \frac{V \cdot C_0 \cdot (1 - e^{-k \cdot \tau})}{M_r \cdot Q_f \cdot 10^{-3} \cdot \tau} \quad (3)$$

where n_{RhB} – amount of Rhodamine B degraded within time τ, mol; n_{RhB} – amount of photons that passed through the reactor within time τ, mol; n_0 – initial amount of Rhodamine B, mol; n – amount of Rhodamine B after τ minutes, mol; C_0 – initial concentration of Rhodamine B, g·L^{-1}; n – concentration of Rhodamine B after τ minutes, g/L; M_{RhB} – molar mass of Rhodamine B, g·mol^{-1}; k – Rhodamine B degradation rate constant, min^{-1}; V – reactor volume, L; τ – reaction time, min.

RESULTS AND DISCUSSION

The initial selection of the suitable counterparts to form a composite was done based on the surface charges of the possible candidates. In this view, poly(heptazine imide) bearing negative surface charge and MIL-125-NH_2 having in part a positively charged surface (see below) seemed to be a suitable pair of semiconductors. The poly(heptazine imide)/MIL-125-NH_2 composites were prepared *in-situ* by simply dispersing both materials in water, and then isolated and characterized. Figure 1A shows the PXRD patterns of PHIK, MIL-125-NH_2 and their composite COM50 which was found to be the most active for Rhodamine B degradation (see below). The characteristic diffraction peaks of MIL-125-NH_2[11] and the two most intense signals of PHIK[9] at 8.1° 2θ and 27.9° 2θ are observed in the pattern of the composite that clearly indicates the presence of both crystalline solids.

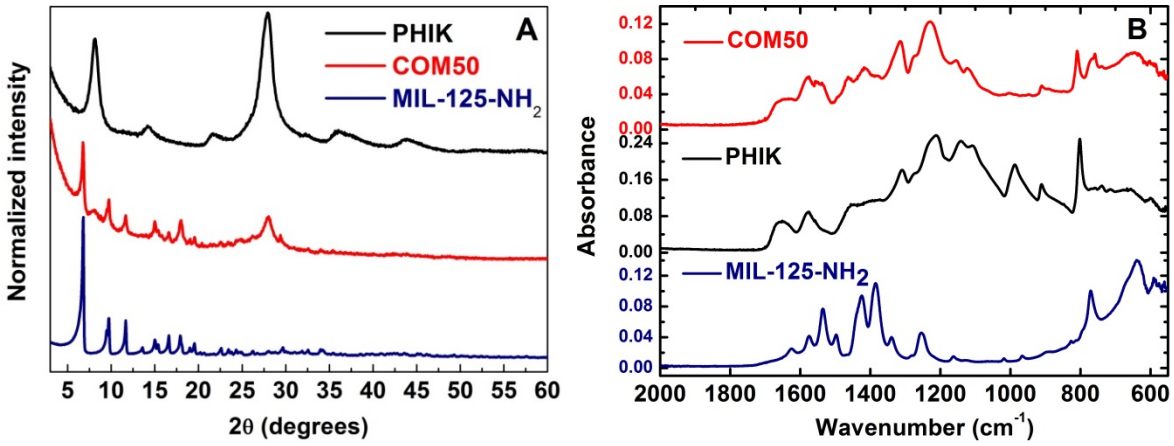

Figure 1. PXRD patterns (A) and FTIR spectra (B) of PHIK (black), COM50 (red) and MIL-125-NH_2 (blue).

Another evidence for composite formation is provided by the comparison of the FTIR spectrum of COM50 with those of pure materials, PHIK and MIL-125-NH_2, as shown in Figure

1B. The spectrum of PHIK exhibits a number of typical vibrations,[22] namely the broad band at 1100–1500 cm^{-1}, composed of the overlapping bands at 1108, 1142, 1212, 1274, 1310, 1392 and 1449 cm^{-1}, which is due to the stretching vibrations of C–N and C=N bonds in the polymer, the band at 802 cm^{-1}, related to the deformation vibrations of tri-*s*-triazine ring, the peaks at 1650 and 1575 cm^{-1}, assigned to N-H bending in H_2NC and HNC_2 groups, respectively, while the absorption bands at 1065 and 987 cm^{-1} are due to the asymmetric and symmetric vibrations of NC_2 bonds, respectively, in metal–NC_2 groups. In the corresponding spectrum of MIL-125-NH_2, absorption peaks at 1497 and 1575 cm^{-1} are due to stretching of C=C bonds in the aromatic ring, strong bands at 1340, 1384, 1424 and 1536 cm^{-1} are due to carboxylate groups, the peak at 1625 cm^{-1} is related to NH bend in NH_2-groups, the one at 1257 cm^{-1} is assigned to CN stretching vibrations, while the strong absorption bands at 770 and 641 cm^{-1} are due to O–Ti–O bonds.[11,23,24] The FTIR spectrum of the composite material contains the characteristic features of both components; however, the majority of the absorption peaks are slightly shifted if compared to their position in the pure materials. The peak of heptazine ring deformation vibrations appears at 808 cm^{-1} in the composite instead of 802 cm^{-1} in PHIK; the O–Ti–O band in the composite is at 760 cm^{-1} compared to 771 cm^{-1} in the original MOF; the vibrations of carboxylate group in the composite are at 1416 and 1379 cm^{-1} instead of 1425 and 1384 cm^{-1} in MIL-125-NH_2. Some peaks only appear to be shifted due to the overlapping of certain bands of pure materials, e.g. the bands at 1315 and 1229 cm^{-1} in the composite are formed from the contributions of PHIK (1310 cm^{-1} and 1212 cm^{-1}) and MIL-125-NH_2 (1340 cm^{-1} and 1257 cm^{-1}). A few peaks remain unchanged upon incorporation of PHIK and MOF into the composite, e.g. those at 1650, 1575 and 1497 cm^{-1} that are due to N-H bending in PHIK and C=C stretching in MIL-125-NH_2. The

observed shifts of the characteristic IR absorption bands suggest that the two compounds interact within the composite.

The most remarkable change, however, is the almost complete disappearance of the PHIK vibrations at 1065 and 987 cm^{-1} that are due to the vibrations of NC_2 bonds of $C_2N^{\ominus}$ K^+ groups, upon formation of the composite. This points to the redistribution of the K^+ ions within the composite and their migration from the poly(heptazine imide) to MOF driven by the higher acidity of the 2-aminoterephthalic acid compared to the imide. Upon migration of K^+ to MOF, PHIK becomes negatively charged, what further strengthens the electrostatic interactions between PHIK and MIL-125-NH_2 (see below) and contributes to the integrity of the composite as illustrated further.

To ensure that the observed changes in the FTIR spectra are related to the composite formation and do not originate from some chemical changes in the pure materials upon their contact with water, both PHIK and MIL-125-NH_2 were dispersed in water, then dried and the FTIR spectra of the resulting products were compared with those of the original solids (Figure S1 A, B). As expected, no chemical changes upon contact with water could be detected.

To reveal the nature of the electronic interactions between the materials within the composite, EPR spectroscopy studies were carried out (Figure 2). Pure solid PHIK shows a single absorption signal with a *g*-value of 2.005, which reveals the presence of localized electrons in its structure even in the dark conditions.[25,26] In the composite, the corresponding signal is slightly shifted to $g = 2.004$ and greatly enhanced indicating that MIL-125-NH_2 induces the production of additional unpaired electrons in PHIK. This fact can be rationalized by the migration of K^+ ions from PHIK to MIL-125-NH_2, in agreement with the FTIR studies.

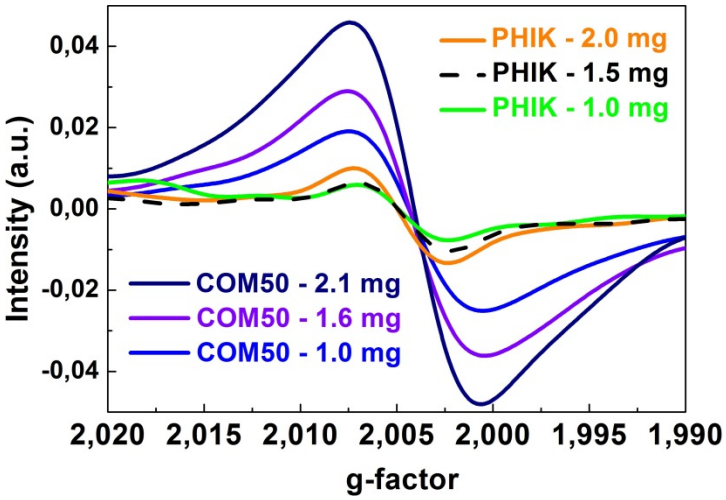

Figure 2. Smoothed EPR spectra of solid potassium poly(heptazine imide), PHIK and composite COM50 measured for different sample weights.

The morphological changes upon the formation of the composite were accessed by scanning electron microscopy (SEM) studies (Figure 3). The pristine PHIK is constituted by micrometric agglomerates covered with nanometric needles (Figure 3A). On the other hand, MIL-125-NH_2 has a disc-like morphology, about 200 nm in diameter and around 50 nm high (Figure 3B). The mixture of PHIK and MIL-125-NH_2 before water treatment (Figure S2) shows the presence of both solids with their typical morphologies. However, the mixture after water treatment exhibits a heterogeneous morphology, represented by nanoparticles of irregular size and shape, and micrometers long layered 'belts' (Figure 3 C, D). The irregular morphology of the sample could be a result of more or less favorable interactions of the materials within the composite, e.g. originating from the different amounts of K^+ ions transferred from PHIK to MIL-125-NH2 and leading to different spatial arrangements. Clearly, the results of SEM studies further support the formation of the composite upon water treatment of PHIK/MIL-125-NH_2 mixtures.

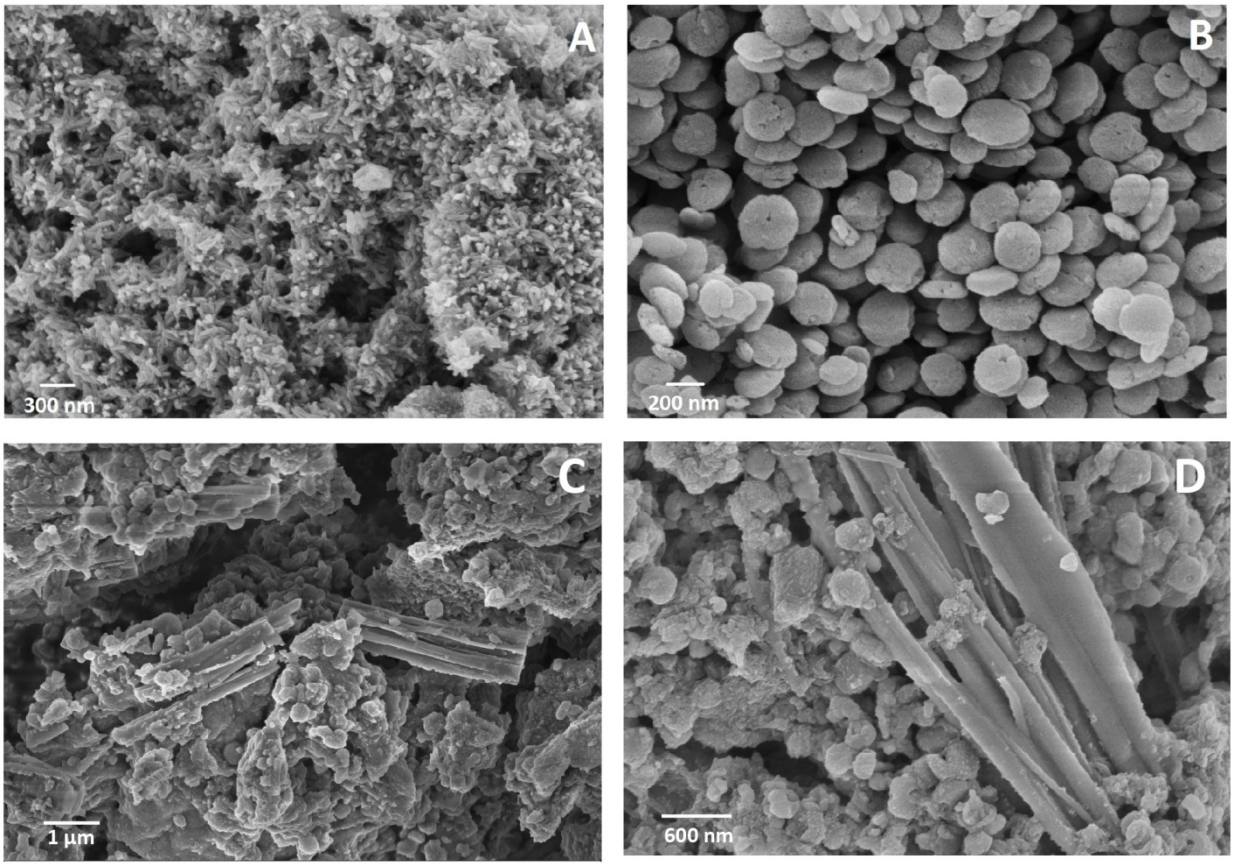

Figure 3. SEM images of PHIK (A), MIL-125-NH_2 (B) and COM50 (C, D).

The N_2 sorption isotherms and the pore size distributions in the starting materials and their composite COM50 are compared in the Figure S3 A and B, respectively. The N_2 isotherm of MIL-125-NH_2 is of type I, reflecting the presence of micropores in the material. A somewhat increased N_2 uptake at p/p_0 close to 1 is an indication of the presence of some macropores. PHIK is a non-porous solid, while the composite exhibits the presence of only few micropores indicating that the major part of micropores is lost upon complex formation. This is probably due to the migration of K^+ ions from PHIK to MIL-125-NH_2 that partially block the micropores. The BET surface areas of MIL-125-NH_2, COM50 and PHIK are 1160, 185 and 30 $m^2 \cdot g^{-1}$, respectively.

For further analysis of the interactions between MIL-125-NH_2 and PHIK, ζ-potential measurements were carried out (Figure 4A). PHIK has a negatively charged surface with –40 mV zeta potential value at pH 6, while MIL-125-NH_2 sample contains both positively and negatively charged particles, with an average zeta potential (–5.41 mV) close to zero. When dispersed in water, positively charged MIL-125-NH_2 particles and PHIK can be attracted together by electrostatic forces and form aggregates.

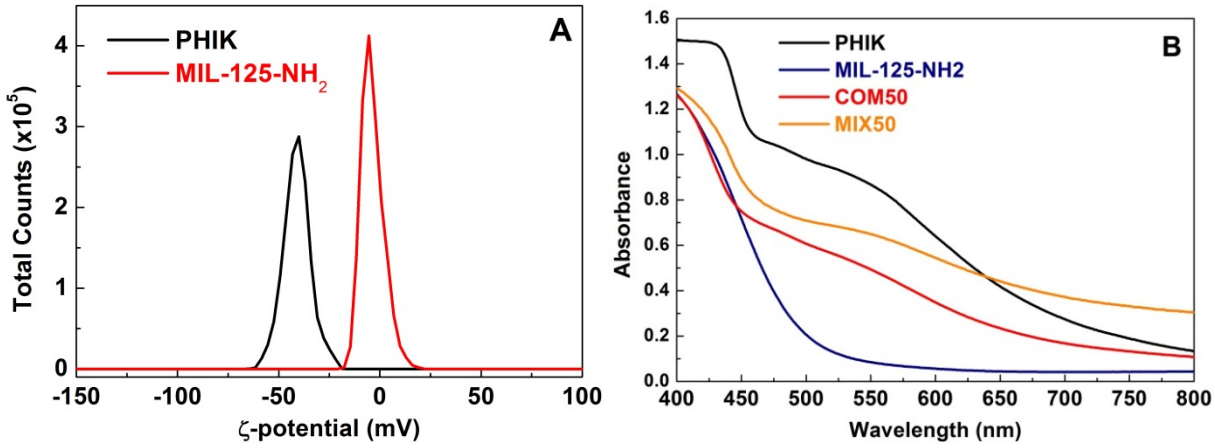

Figure 4. Zeta-potential distributions (A) of PHIK (black) and MIL-125-NH_2 dispersed in water at pH 6 (red). UV/Visible absorption spectra (B) of PHIK (black), COM50 (red), MIX50 (orange) and MIL-125-NH_2 (blue).

Summarizing, FTIR and EPR measurements unequivocally show that K^+ ions migrate from PHIK to MIL-125-NH_2, while SEM studies illustrate the changes of morphology of PHIK/MOF mixture after being dispersed in water. Based on the fact that ζ-potential measurements show that a fraction of MIL-125-NH_2 particles have a slight positive charge, we assume that those positively charged MIL-125-NH_2 species can interact electrostatically with the negatively charged PHIK (Scheme 1, step 1). Upon the contact of the two materials, the migration of K^+ ions from PHIK to MIL-125-NH_2 (Scheme 1, step 2) makes PHIK more negatively charged, in

agreement with EPR data (see above), while MIL-125-NH_2 becomes more positively charged further enhancing the electrostatic interactions between the solids. Probable chemical bonds at the interface of the two materials are depicted in Scheme S1. Negatively charged and neutral MIL-125-NH_2 particles can approach and contact PHIK or MOF particles due to their high kinetic energy provided by agitation and electrostatic attraction to positively charged MIL-125-NH_2 particles (Scheme 1, step 2). Upon the contact of the solids, a migration of additional K^+ ions from PHIK to MIL-125-NH_2 becomes possible, further strengthening the electrostatic interactions in the composite (Scheme 1, step 3). The quantitative diffusion of K^+ ions from PHIK to MOF would provide the strongest interaction between PHI and MOF in the complex (Scheme 1, step 4).

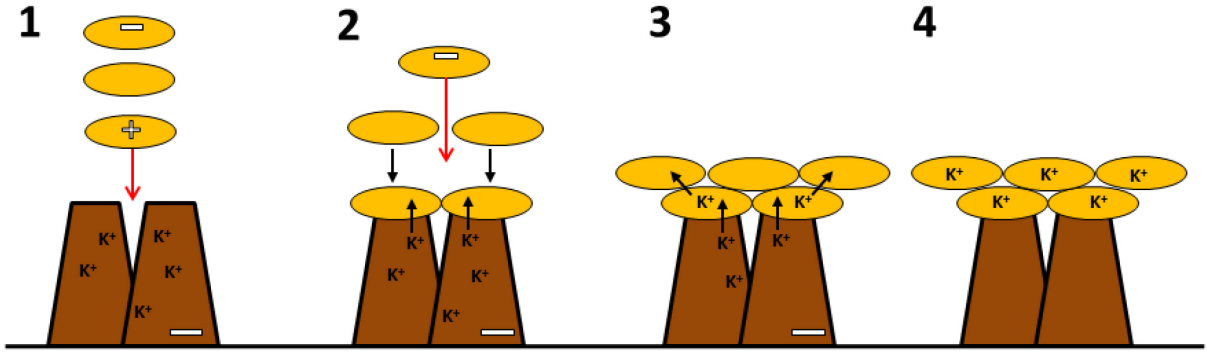

Scheme 1. Proposed mechanism of the composite formation. Step 1 shows the approach of MIL-125-NH_2 (yellow disks) to PHIK (brown tetrahedron) by electrostatic forces (red arrow). Step 2 shows the diffusion (black arrow) of K^+ ions to MIL-125-NH_2. Other MIL-125-NH_2 particles, neutral or negatively charged, can approach the surface of PHIK due to their high kinetic energy provided by agitation and electrostatic attraction to positively charged MIL-125-NH_2 particles. Step 3 shows the diffusion of additional K^+ ions to MIL-125-NH_2. Step 4 shows the state of the final composite with K^+ ions inside the micropores of MIL-125-NH_2.

Optical absorption properties of PHIK, MIL-125-NH_2, their mechanical mixture MIX50 and the composite COM50 are depicted in Figure 4B. The absorption thresholds of MIL-125-NH_2 and PHIK are approximately 525 nm and 750 nm, respectively. The visible light absorption of the MOF originates from the O to Ti charge transfer in $TiO_5(OH)$ inorganic clusters influenced by 2-aminoterephthalate ligands.[12] The two absorption bands in PHIK spectra at $\lambda < 450$ nm and $\lambda \sim 525$ nm are due to $\pi \rightarrow \pi^*$ electron transitions in the conjugated aromatic ring system and $n \rightarrow \pi^*$ transitions involving lone pairs of the edge nitrogen atoms of the heptazine ring, respectively.[9,27] The bandgaps of the pure materials were estimated from the Tauc plots, depicted in Figure S4. The corresponding values for PHIK and MIL-125-NH_2 are 1.9 eV and 2.6 eV, respectively, in agreement with previous reports.[9,11] In the spectrum of COM50, the absorption threshold of the first absorption band is blue-shifted compared to the mixture and also to pure MIL-125-NH_2 that points to the slight modification of the electronic properties of materials upon composite formation. The absorbances of PHIK, COM50 and MIL-125-NH_2 in the wavelength range of 465±30 nm that corresponds to the blue LED emission spectrum used in photocatalytic experiments (see below) are related as 1:0.628:0.500.

The photocatalytic activity of the pure materials was compared with the performance of the MOF/PHIK composites in the decoloration of Rhodamine B under blue light irradiation ($\lambda = 465$ nm). This first step of Rhodamine B degradation can be due to de-ethylation of the dye molecule and/or direct oxidation of the chomophore structure.[3,28-30] The detailed studies of the mechanism of Rhodamine B photodegradation are beyond the scope of the present contribution; and the interested reader is encouraged to refer to the dedicated literature.[31–33] Figure 5A shows the decrease of RhB relative concentrations (C/C_0) with the irradiation time in the presence of PHIK, MIL-125-NH_2, and their composites, COM25, COM50 and COM75 as photocatalysts, while

Figure 5B depicts the corresponding values of the calculated rate constants. Both MOF and PHIK are found to degrade RhB with the rate constants k = 0.010 and k = 0.003 min^{-1}, respectively, however, COM50 shows twice higher activity (k = 0.020 min^{-1}) compared to MIL-125-NH_2 and is seven times more active than PHIK alone.

Apparent quantum efficiencies of the photocatalysts could be determined knowing the value of a photon flux through the reactor (see Equation (1), Experimental Section), which was measured using potassium ferrioxalate as a standard chemical actinometer.[34,35] The apparent quantum efficiencies ($\boldsymbol{\varphi_x}$) calculated according to Equation (3) (see Experimental Section for the details)[21] are $9.1 \cdot 10^{-5}$, $3.9 \cdot 10^{-5}$ and $11.8 \cdot 10^{-5}$ for MIL-125-NH_2, PHIK and COM50, respectively. These values indicate that COM50 is 30 % more efficient than the MOF and 3 times more efficient than PHIK. The low values of $\boldsymbol{\varphi_x}$ are explained by the two factors. Firstly, the calculations were done assuming that the degradation of Rhodamine B is a one electron/hole process. This is, of course, not true, and much greater number of the photogenerated charge carriers participate in the complex mechanism of the dye degradation. Secondly, apparent quantum efficiency does not take into account the fraction of light absorbed by the photocatalyst, especially considering the presence of a dye in the reaction mixture, and therefore is in fact a lower limit on the true quantum yield.[21]

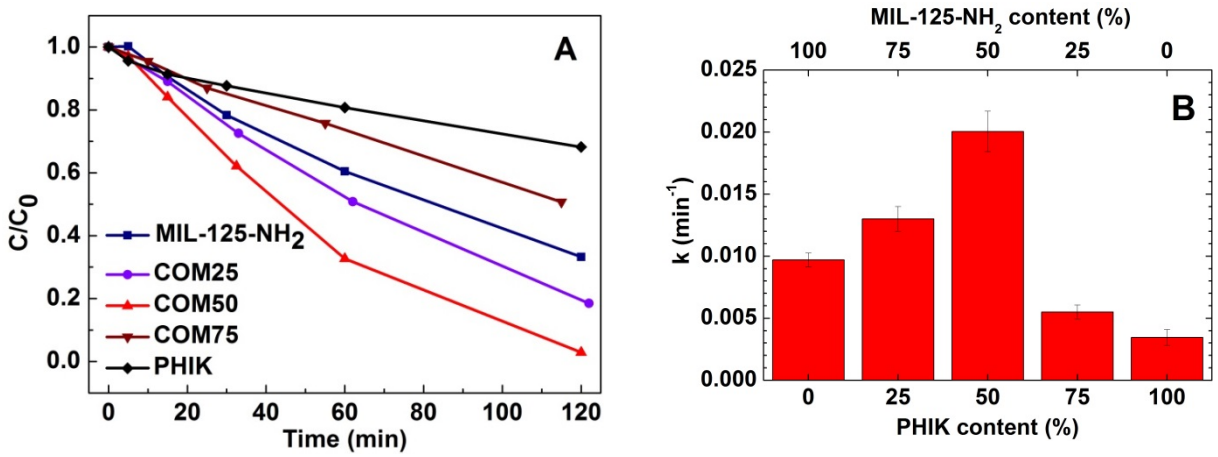

Figure 5. Degradation of RhB by MIL-125-NH_2 (blue), PHIK (black), COM25 (violet), COM50 (red) and COM75 (brown) (A). Calculated rate constants of RhB degradation using PHIK/MIL-125-NH_2 photocatalyst as a function of its composition (B).

To rationalize the synergistic effect of PHIK and MIL-125-NH_2 within the composite in RhB degradation reaction, the electronic structures of the materials should be considered. The electrochemical impedance spectroscopy and Mott-Schottky analysis were used to determine the band structure of MIL-125-NH_2 (Figure S5). The flat-band potential of MIL-125-NH_2 is found to be -0.63 V (vs. Normal Hydrogen Electrode, NHE). Since it behaves as an *n*-type semiconductor, given the positive slope of the Mott-Schottky plot, we conclude that its conduction band (CB) is located at about -0.63 V (vs. NHE). Thereby, the valence band (VB) of MIL-125-NH_2 is located at 1.97 V (vs. NHE). The comparison of the CB positions of the MOF (E_{CB} = -0.63 V) and PHIK (E_{CB} = -0.21 V (vs. RHE at pH =7) = -0.62 V (vs. NHE)[9]) suggests that the photogenerated electrons can be transferred from MIL-125-NH2 to PHIK. Besides, the similarity of the CB potentials of the two materials may facilitate this charge transfer. In general, PHIK/MIL-125-NH_2 composite has a type-I heterostructure.[1,2] In such composites, the conduction and valence band of the material with the smaller bandgap (PHIK in this case) are located between the CB

and VB levels of the solid with the larger bandgap (MIL-125-NH_2). The consequence of such positioning of bands is that both holes and electrons are thermodynamically allowed to migrate from MIL-125-NH_2 to PHIK.

To get deeper insight into the electron transfer processes in pure materials and in COM50, EPR measurements of the irradiated anaerobic suspensions of the solids in the presence of triethanolamine (TEOA), an effective hole scavenger, were carried out. Such a procedure typically leads to the accumulation of electrons in the semiconductors provided that no oxygen or other electron acceptor is present in the solution. The electrons accumulated under blue light irradiation in the metallic oxo-clusters of MIL-125-NH_2 sample, produce a photochromic effect in which yellow MIL-125-NH_2 turns green.[12] This photochromic effect is caused by the formation of Ti(III) species that can be detected by EPR spectroscopy at room temperature as a broad signal at g = 1.944, as shown in Figure 6A. However, no signal at g = 1.944 is observed in COM50, suggesting that Ti (III) states are not present in the composite. This result confirms the existence of a charge transfer of photogenerated electrons from MIL-125-NH_2 to PHIK. On the other hand, upon irradiation of PHIK in the presence of the hole scavenger, numerous localized photoexcited electrons are accumulated under blue and green light excitation in its conduction band as suggested by the extraordinary intense and sharp signal at g = 2.008 (Figure 6B). The accumulation of the electrons is also accompanied by a significant photochromic effect leading to the darkening of the solid as illustrated in Figure S6. The darkening of PHIK is reversible, and the original state of the material is easily recovered upon its exposure to air, that leads to scavenging of the accumulated electrons by O_2 molecules. Remarkably, in the case of COM50, the intensity of the signal at g = 2.008 is significantly smaller compared to pure PHIK under both blue and green light illumination. The fact that COM50 does not accumulate electrons under the

green light irradiation (which is only absorbed by PHIK solid in the MIL-125-NH_2/PHIK composite) and under the blue light irradiation (which is absorbed by both components) probably implies that TEOA is unable to remove holes from PHIK (and MIL-125-NH_2) efficiently, when they are incorporated in the composite. As we discussed above, PHIK and MOF interact strongly within the composite (electrostatically, by H-bonding), thus PHIK – TEOA interactions may be significantly weakened. Moreover, sterically hindered access of TEOA to PHIK solid partially surrounded by MIL-125-NH_2, may be further responsible for weakening of TEOA – PHIK interactions.

Depending on the relative mobilities of the photogenerated electrons and holes within MIL-125-NH_2, two possible explanations are suggested to explain the enhanced photocatalytic activity of the COM50 and the relatively small EPR signal at g = 2.008 in COM50 under blue light irradiation, when MIL-125-NH_2 does transfer its photogenerated electrons to PHIK, as discussed above. Some recent kinetics studies on other semiconductors, such as TiO_2 and ZnS, have shown that the times of electron transfer at the surface of the photoexcited semiconductor at pH 7 are typically smaller than the times of the hole loss.[36–38] This can be considered as an indirect evidence of the higher migration rates of the electrons compared to holes. However, since no kinetic data are available for PHIK and MIL-125-NH_2 so far, below we describe both possibilities.

If the relative mobilities of the charge carriers have comparable rates, both electrons and holes photogenerated in MIL-125-NH_2 are transferred to PHIK. The low EPR signal in COM50 may be then due to the fact that TEOA cannot remove holes from PHIK efficiently, e.g. due to steric hindrance of weakened interactions. Thus, the recombination of charge carriers in PHIK prevents the accumulation of electrons.

If the mobility of the electrons in the MOF is higher than that of the holes, electrons will be transferred to PHIK, while holes will stay in MIL-125-NH_2, thus leading to a charge separation within the composite. The electrons transferred from the CB of MIL-125-NH_2 to the CB of PHIK may cause the overpopulation of the latter and induce recombination of the electrons with the holes present in the VB of PHIK, while the remaining holes in the VB of MOF are efficiently scavenged by TEOA. In this way, MIL-125-NH_2 partially suppresses the accumulation of charges in the composite. That would explain the fact why the intensities of the EPR signals of the COM50 upon 470 and 530 nm irradiation are almost the same, while the EPR signal of PHIK at 470-nm irradiation is significantly more intense compared to the one under 530 nm irradiation.

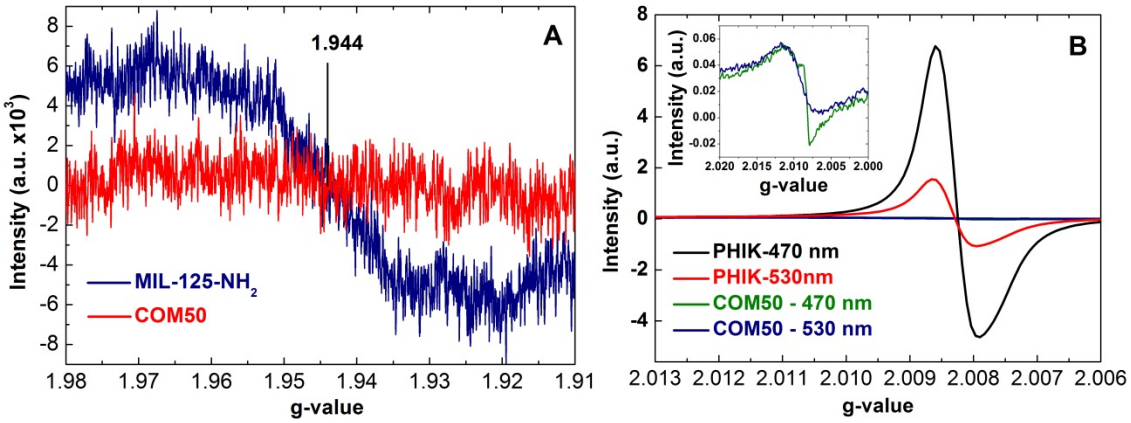

Figure 6. EPR spectra of MIL-125-NH_2 (blue) and COM50 (red) after irradiation in the anaerobic solution of TEOA (A). EPR spectra of the irradiated samples of PHIK (black for 470 nm and red for 530nm) and COM50 (green for 470 nm and blue for 530 nm) in an anaerobic solution of TEOA (B). EPR spectra in (A) and (B) are shown for different g-values to distinguish between the signals of the electrons accumulated at Ti(III) centers (A) and in PHIK(B).

Knowing the electronic structure of the composite, we can try to rationalize the increase of RhB degradation rates in the presence of semiconductor composites in comparison to the reaction rates observed using pure materials as catalysts. RhB can be oxidized by a sensitization

mechanism[3] or directly by photogenerated holes. The formation of $HO^{\bullet}$ radicals is thermodynamically forbidden, due to the fact that the valence band potentials of both materials are less positive than required for hydroxyl radical formation (E (H^+, $HO^{\bullet}/H_2O$) vs. NHE) = 2.75 – 0.06 pH = 2.33 V at pH=7).[39] However, considering that the reduction potential of RhB^+/RhB couple (1.36V vs. NHE)[40] is less positive than the valence band potential of MIL-125-NH_2 (1.97 V vs. NHE), the oxidation of RhB by the holes photogenerated in MIL-125-NH_2 is also probable. The VB potential of PHIK (1.28V vs. NHE) is close to the redox potential of RhB, but is less positive, thus oxidation of RhB in its ground state by the holes photogenerated in PHIK is thermodynamically unfavorable. This may be responsible for a relatively low degradation rate of RhB in the presence of PHIK as a photocatalyst. The activity of pure PHIK in RhB degradation would be then explained either by degradation of excited dye molecules (RhB*) with $O_2^{\bullet-}$ radicals or by direct oxidation of RhB* by the holes in PHIK (see below), or the combination of both.

As already mentioned above, depending on the relative mobilities of the charge carriers in the MOF, we suggest two possible mechanisms to explain better photocatalytic performance of COM50 compared to the pure materials. For the case, when both electrons and holes can be simultaneously transferred from MIL-125-NH_2 to PHIK, a dye sensitization mechanism is suggested as the main pathway for RhB degradation, since holes in MIL-125-NH_2 would not be available to oxidize RhB. Indeed, the excitation energy of the dye is E_{00} = 2.18eV, and under the experimental conditions used the absorbance of RhB is 0.7 at 465 nm (Figure S7). Thus, dye oxidation *via* electron injection from the excited dye to PHIK and MIL-125-NH_2 is feasible, as the reduction potential of RhB^+/ RhB* (-0.83 V vs. NHE)[41] (Figure 7) is more negative than the CB potentials of both materials. Namely, the excitation of the dye gives rise to RhB* that injects

an electron in CB of MIL-125-NH_2, and the generated RhB^+ cations undergo self-oxidation. The increase of the dye degradation rates in the presence of the composite is ascribed to the electron transfer from MIL-125-NH_2 to PHIK, which inhibits electron back-transfer (RhB^+ could, in principle, retake the electrons from the CB of MIL-125-NH_2 and get reduced to RhB ground state).

In the case, when only electrons are transferred to PHIK, irradiation of the composite leads to a charge separation, and the excess of holes in the VB of MIL-125-NH_2 degrades additional RhB molecules. Thus, the increase of the reaction rate is observed.

Finally, dissolved O_2 removes electrons from PHIK, giving $O_2^{\bullet-}$ radicals, which can also oxidize the dye (see Figure 7). According to the obtained kinetic data, the optimal charge transfer from MIL-125-NH_2 to PHIK is reached at 1:1 components ratio.

The summary of the possible degradation pathways explaining, why the composite (COM50) degrades RhB faster than the pure materials, are depicted in Figure 7.

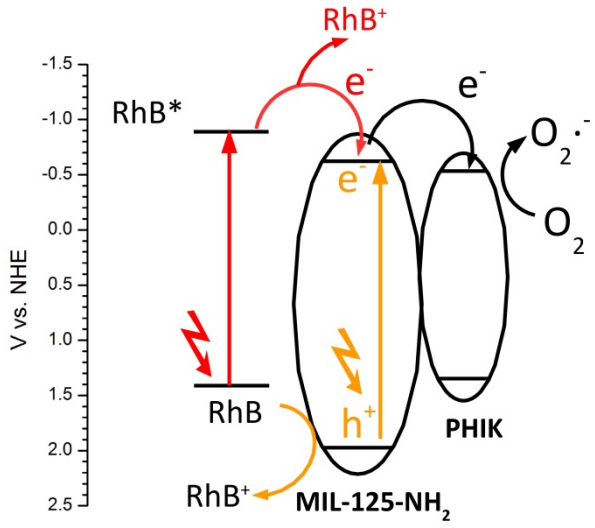

Figure 7. Possible explanations of the enhanced RhB degradation activity by the composite. The scheme depicts the energy levels of conduction and valence bands of MIL-125-NH_2 and PHIK. The pathway involving the oxidation of RhB by holes in MIL-125-NH_2 is depicted with orange

arrows and letters. The mechanism involving the injection of electrons from RhB* towards MIL-125-NH_2 is shown with red arrows and letters. The shared steps of electron transfer from MIL-125-NH_2 to PHIK and scavenging of electrons by oxygen is depicted with black arrows and letters. The actual excitation of PHIK by visible light is not shown for clarity, since it is not considered as being responsible for the enhanced composite activity.

CONCLUSIONS

We have discovered a facile route to prepare composite photocatalysts composed of PHIK and MIL-125-NH_2. Potentially, this strategy can be applied to the synthesis of others PHIK/MOF composites, provided that the solids attract each other (at least partially), for example by given possibility of other MOFs to accommodate K^+ ions in their micropores. The obtained type I heterostructure exhibits a synergistic effect for RhB degradation through an efficient electron transfer from the MOF to PHIK. Two explanations are suggested depending on the relative mobilities of the photogenerated charge carriers in MIL-125-NH_2. If the mobilities of the electrons and holes are similar, both types of the charge carriers are transferred from the MOF to PHIK. The enhancement of the activity is then due to the electron injection from the RhB* to MOF and the suppression of the electron transfer back to RhB* by their forward transfer to PHIK. If the mobility of the electrons in the MOF is higher than that of the holes, electrons (only) are transferred to PHIK where they can reduce O_2 molecules producing additional $O_2^{\bullet-}$ radicals able to oxidize RhB. At the same time, the excess of holes in the MIL-125-NH_2 is oxidizing additional RhB molecules. Overall, the increased reaction rates are due to an efficient charge separation within the composite.

ASSOCIATED CONTENT

Supporting Information. FTIR spectra of MIL-125-NH_2 before and after water treatment, SEM image of the mixture of MIL-125-NH_2 and PHIK before water treatment, illustration of possible chemical interactions at MOF/PHI interface, N_2 sorption isotherms and pore size distributions in solids, Tauc plots for MIL-125-NH_2 and PHIK, Mott-Schottky plot for MIL-125-NH_2, images depicting the photochromic effect in PHIK, absorption spectrum of a Rhodamine B solution. The Supporting Information file is available free of charge at http://pubs.acs.org.

AUTHOR INFORMATION

Corresponding Author

*Dariya Dontsova: dariya.dontsova@mpikg.mpg.de

*María A. Grela: magrela@mdp.edu.ar

Funding Sources

Research fundings from ANPCyT (Agencia Nacional de Promocion Cientifica y Tecnica, Argentina) to M.A.G. under project 1456 are gratefully acknowledged. This work was also made possible by a Bunge & Born Foundation-Max Planck Society scholarship.

Notes

The authors declare no competing financial interest.

ACKNOWLEDGMENT

N.A.R. acknowledges Bunge & Born Foundation and Max Planck Society for its “Doctorate Grant Fundación Bunge y Born – Max Planck – 2016” to conduct this work at Max Planck Institute of Colloids and Interfaces. N.A.R. acknowledges CONICET for his doctoral fellowship. Dr. Matías Valdés is acknowledged for the electrochemical measurement. M.A.G. is member of

the research staff of CONICET, Argentina. Special thanks to Dr. Bogdan Kupril for the fruitful discussions.

REFERENCES

(1) Marschall, R. Semiconductor Composites: Strategies for Enhancing Charge Carrier Separation to Improve Photocatalytic Activity. *Adv. Funct. Mater.* **2014**, *24*, 2421–2440.

(2) Sudha, D.; Sivakumar, P. Review on the Photocatalytic Activity of Various Composite Catalysts. *Chem. Eng. Process.* **2015**, *97*, 112–133.

(3) Wang, H.; Yuan, X.; Wu, Y.; Zeng, G.; Chen, X.; Leng, L.; Li, H. Synthesis and Applications of Novel Graphitic Carbon Nitride/metal-Organic Frameworks Mesoporous Photocatalyst for Dyes Removal. *Appl. Catal., B* **2015**, *174–175*, 445–454.

(4) Wang, S.; Lin, J.; Wang, X. Semiconductor–redox Catalysis Promoted by Metal–organic Frameworks for CO_2 Reduction. *Phys. Chem. Chem. Phys.* **2014**, *16*, 14656–14660.

(5) Zhou, H.; Li, P.; Liu, J.; Chen, Z.; Liu, L.; Dontsova, D.; Yan, R.; Fan, T.; Zhang, D.; Ye, J. Biomimetic Polymeric Semiconductor Based Hybrid Nanosystems for Artificial Photosynthesis towards Solar Fuels Generation via CO_2 Reduction. *Nano Energy* **2016**, *25*, 128–135.

(6) Maeda, K.; Wang, X.; Nishihara, Y.; Lu, D.; Antonietti, M.; Domen, K. Photocatalytic Activities of Graphitic Carbon Nitride Powder for Water Reduction and Oxidation under Visible Light. *J. Phys. Chem. C* **2009**, *113*, 4940–4947.

(7) Martin, D. J.; Reardon, P. J. T.; Moniz, S. J. A.; Tang, J. Visible Light-Driven Pure Water Splitting by a Nature-Inspired Organic Semiconductor-Based System. *J. Am. Chem. Soc.*

2014, *136*, 12568–12571.

(8) Xu, J.; Brenner, T. J. K.; Chabanne, L.; Neher, D.; Antonietti, M.; Shalom, M. Liquid-Based Growth of Polymeric Carbon Nitride Layers and Their Use in a Mesostructured Polymer Solar Cell with V_{oc} Exceeding 1 V. *J. Am. Chem. Soc.* **2014**, *136*, 13486–13489.

(9) Dontsova, D.; Pronkin, S.; Wehle, M.; Chen, Z.; Fettkenhauer, C.; Clavel, G.; Antonietti, M. Triazoles: A New Class of Precursors for the Synthesis of Negatively Charged Carbon Nitride Derivatives. *Chem. Mater.* **2015**, *27*, 5170–5179.

(10) Rodríguez, N. A.; Parra, R.; Grela, M. A. Structural Characterization, Optical Properties and Photocatalytic Activity of MOF-5 and Its Hydrolysis Products: Implications on Their Excitation Mechanism. *RSC Adv.* **2015**, *5*, 73112–73118.

(11) Hendon, C. H.; Tiana, D.; Fontecave, M.; Sanchez, C.; D'arras, L.; Sassoye, C.; Rozes, L.; Mellot-Draznieks, C.; Walsh, A. Engineering the Optical Response of the Titanium-MIL-125 Metal–Organic Framework through Ligand Functionalization. *J. Am. Chem. Soc.* **2013**, *135*, 10942–10945.

(12) Fu, Y.; Sun, D.; Chen, Y.; Huang, R.; Ding, Z.; Fu, X.; Li, Z. An Amine-Functionalized Titanium Metal-Organic Framework Photocatalyst with Visible-Light-Induced Activity for CO_2 Reduction. *Angew. Chem., Int. Ed.* **2012**, *51*, 3364–3367.

(13) Wang, W.; Huang, X.; Wu, S.; Zhou, Y.; Wang, L.; Shi, H.; Liang, Y.; Zou, B. Preparation of p-n Junction $Cu_2O/BiVO_4$ Heterogeneous Nanostructures with Enhanced Visible-Light Photocatalytic Activity. *Appl. Catal., B* **2013**, *134–135*, 293–301.

(14) Sivula, K.; Formal, F. Le; Grätzel, M. WO_3−Fe_2O_3 Photoanodes for Water Splitting: A

Host Scaffold, Guest Absorber Approach. *Chem. Mater.* **2009**, *21*, 2862–2867.

(15) Xu, J.; Cao, X. Characterization and Mechanism of MoS_2/CdS Composite Photocatalyst Used for Hydrogen Production from Water Splitting under Visible Light. *Chem. Eng. J.* **2015**, *260*, 642–648.

(16) Cetinkaya, T.; Neuwirthová, L.; Kutláková, K. M.; Tomášek, V.; Akbulut, H. Synthesis of Nanostructured TiO_2/SiO_2 as an Effective Photocatalyst for Degradation of Acid Orange. *Appl. Surf. Sci.* **2013**, *279*, 384–390.

(17) Li, W.; Wu, D.; Yu, Y.; Zhang, P.; Yuan, J.; Cao, Y.; Cao, Y.; Xu, J. Investigation on a Novel ZnO/ TiO_2–B Photocatalyst with Enhanced Visible Photocatalytic Activity. *Phys. E Low-dimensional Syst. Nanostructures* **2014**, *58*, 118–123.

(18) Hamid, S. B. A.; Tan, T. L.; Lai, C. W.; Samsudin, E. M. Multiwalled Carbon nanotube/ TiO_2 Nanocomposite as a Highly Active Photocatalyst for Photodegradation of Reactive Black 5 Dye. *Chin. J. Catal.* **2014**, *35*, 2014–2019.

(19) Leghari, S. A. K.; Sajjad, S.; Chen, F.; Zhang, J. WO_3/TiO_2 Composite with Morphology Change via Hydrothermal Template-Free Route as an Efficient Visible Light Photocatalyst. *Chem. Eng. J.* **2011**, *166*, 906–915.

(20) Perales-Martínez, I. A.; Rodríguez-González, V.; Lee, S.; Obregón, S. Facile Synthesis of $InVO_4$/TiO_2 Heterojunction Photocatalysts with Enhanced Photocatalytic Properties under UV–vis Irradiation. *J. Photochem. Photobiol., A* **2015**, *299*, 152–158.

(21) Buriak, J. M.; Kamat, P. V.; Schanze, K. S. Best Practices for Reporting on Heterogeneous Photocatalysis. *ACS Appl. Mater. Interfaces* **2014**, *6*, 11815–11816.

(22) Savateev, A.; Pronkin, S.; Epping, J. D.; Willinger, M. G.; Wolff, C.; Neher, D.; Antonietti, M.; Dontsova, D. Potassium Poly(heptazine Imides) from Aminotetrazoles: Shifting Band Gaps of Carbon Nitride-like Materials for More Efficient Solar Hydrogen and Oxygen Evolution. *ChemCatChem* **2017**, *9*, 167–174.

(23) Jin, D.; Xu, Q.; Yu, L.; Hu, X. Photoelectrochemical Detection of the Herbicide Clethodim by Using the Modified Metal-Organic Framework Amino-MIL-125(Ti)/TiO_2. *Microchim. Acta* **2015**, *182*, 1885–1892.

(24) Abdelhameed, R. M.; Simões, M. M. Q.; Silva, A. M. S.; Rocha, J. Enhanced Photocatalytic Activity of MIL-125 by Post-Synthetic Modification with Cr^{III} and Ag Nanoparticles. *Chem. - Eur. J.* **2015**, *21*, 11072–11081.

(25) Ho, W.; Zhang, Z.; Xu, M.; Zhang, X.; Wang, X.; Huang, Y. Enhanced Visible-Light-Driven Photocatalytic Removal of NO: Effect on Layer Distortion on g-C_3N_4 by H_2 Heating. *Appl. Catal., B* **2015**, *179*, 106–112.

(26) Sano, T.; Tsutsui, S.; Koike, K.; Hirakawa, T.; Teramoto, Y.; Negishi, N.; Takeuchi, K. Activation of Graphitic Carbon Nitride (g-C_3N_4) by Alkaline Hydrothermal Treatment for Photocatalytic NO Oxidation in Gas Phase. *J. Mater. Chem. A* **2013**, *1*, 6489–6496.

(27) Jorge, A. B.; Martin, D. J.; Dhanoa, M. T. S.; Rahman, A. S.; Makwana, N.; Tang, J.; Sella, A.; Corà, F.; Firth, S.; Darr, J. A.; McMillan, P. F. H_2 and O_2 Evolution from Water Half-Splitting Reactions by Graphitic Carbon Nitride Materials. *J. Phys. Chem. C* **2013**, *117*, 7178–7185.

(28) Yuan, X.; Wang, H.; Wu, Y.; Zeng, G.; Chen, X.; Leng, L.; Wu, Z.; Li, H. One-Pot Self-

Assembly and Photoreduction Synthesis of Silver Nanoparticle-Decorated Reduced Graphene Oxide/MIL-125(Ti) Photocatalyst with Improved Visible Light Photocatalytic Activity. *Appl. Organomet. Chem.* **2016**, *30*, 289–296.

(29) Zhu, S.-R.; Liu, P.-F.; Wu, M.-K.; Zhao, W.-N.; Li, G.-C.; Tao, K.; Yi, F.-Y.; Han, L. Enhanced Photocatalytic Performance of BiOBr/NH_2-MIL-125(Ti) Composite for Dye Degradation under Visible Light. *Dalt. Trans.* **2016**, *45*, 17521–17529.

(30) Wu, T.; Liu, G.; Zhao, J.; Hidaka, H.; Serpone, N. Photoassisted Degradation of Dye Pollutants. V. Self-Photosensitized Oxidative Transformation of Rhodamine B under Visible Light Irradiation in Aqueous TiO_2 Dispersions. *J. Phys. Chem. B* **1998**, *102*, 5845–5851.

(31) He, Z.; Sun, C.; Yang, S.; Ding, Y.; He, H.; Wang, Z. Photocatalytic Degradation of Rhodamine B by Bi_2WO_6 with Electron Accepting Agent under Microwave Irradiation: Mechanism and Pathway. *J. Hazard. Mater.* **2009**, *162*, 1477–1486.

(32) Yang, Y.; Guo, Y.; Hu, C.; Jiang, C.; Wang, E. Synergistic Effect of Keggin-Type $[X^{n+}W_{11}O_{39}]^{(12-n)-}$ and TiO_2 in Macroporous Hybrid Materials $[X^{n+}W_{11}O_{39}]^{(12-n)-}$–$TiO_2$ for the Photocatalytic Degr. *J. Mater. Chem.* **2003**, *13*, 1686–1694.

(33) Bhowmik, T.; Kundu, M. K.; Barman, S. Ultra Small Gold Nanoparticles–graphitic Carbon Nitride Composite: An Efficient Catalyst for Ultrafast Reduction of 4-Nitrophenol and Removal of Organic Dyes from Water. *RSC Adv.* **2015**, *5*, 38760–38773.

(34) Hatchard, C. G.; Parker, C. A. A New Sensitive Chemical Actinometer. II. Potassium Ferrioxalate as a Standard Chemical Actinometer. *Proc. R. Soc. A* **1956**, *235*, 518–536.

(35) Sauers, R. R.; Van Arnum, S. D.; Scimone, A. A. Green Chemistry Analytical Method Development: A Revisit on the Use of Potassium Ferrioxalate as a Chemical Actinometer. *Green Chem.* **2004**, *6*, 578–582.

(36) Cornu, C. J. G.; Colussi, A. J.; Hoffmann, M. R. Time Scales and pH Dependences of the Redox Processes Determining the Photocatalytic Efficiency of TiO_2 Nanoparticles from Periodic Illumination Experiments in the Stochastic Regime. *J. Phys. Chem. B* **2003**, *107*, 3156–3160.

(37) Zhou, R.; Guzman, M. I. CO_2 Reduction under Periodic Illumination of ZnS. *J. Phys. Chem. C* **2014**, *118*, 11649–11656.

(38) Zhou, R.; Guzman, M. I. Photocatalytic Reduction of Fumarate to Succinate on ZnS Mineral Surfaces. *J. Phys. Chem. C* **2016**, *120*, 7349–7357.

(39) Wardman, P. Reduction Potentials of One-Electron Couples Involving Free Radicals in Aqueous Solution. *J. Phys. Chem. Ref. Data* **1989**, *18*, 1637–1755.

(40) Huang, J.; Stockwell, D.; Boulesbaa, A.; Guo, J.; Lian, T. Comparison of Electron Injection Dynamics from Rhodamine B to In_2O_3, SnO_2, and ZnO Nanocrystalline Thin Films. *J. Phys. Chem. C* **2008**, *112*, 5203–5212.

(41) Hashimoto, K.; Hiramoto, M.; Sakata, T. Temperature-Independent Electron-Transfer: Rhodamine B/oxide Semiconductor Dye-Sensitization System. *J. Phys. Chem.* **1988**, *92*, 4272–4274.

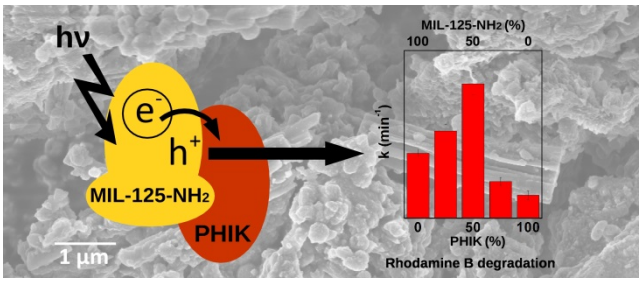
hν
e-
h+
MIL-125-NH2
PHIK
1 μm
MIL-125-NH2 (%)
100 50 0
k (min-1)
0 50 100
PHIK (%)
Rhodamine B degradation